Article ID：1007−7294(2026)06−0925−15

Numerical Analysis of Overload/Underload Effect on Fatigue Crack Propagation Behavior of AH32 Steel

DONG Qin[1], *DAI Qian−sheng*[2], *MAO Yi−xin*[2], *HU Yao−yu*[3], *QIN Kai*[1]

(1. Key Laboratory of High Performance Ship Technology (Wuhan University of Technology), Ministry of Education, Wuhan 430063, China; 2. School of Naval Architecture, Ocean and Energy Power Engineering, Wuhan University of Technology. Wuhan 430063, China; 3. Marine Equipment and Technology Institute, Jiangsu University of Science and Technology, Zhenjiang 212003, China)

Abstract: This paper investigates the effects of different overload conditions on crack propagation behavior of AH32 steel, including tensile overload ratios, overload-underload, underload-overload and underload. The residual stress distribution in the region near the crack tip under different overload ratios and overload conditions all result from plastic deformation of the material near the crack tip during fatigue crack propagation. It is shown that applying tensile overload postpones the crack growth, while underload promotes the crack growth. Furthermore, it is also observed that the crack closure level shows a fast increase with the increase of overload ratio. Finally, it can be seen that the mechanism of residual stress at the crack tip and the mechanism of plastic deformation at the crack tip controlling the transient crack growth behavior under variable amplitude loading are essentially the same.

Key words: overload; retardation effect; crack growth; crack closure; AH32 steel

CLC number: U668.2 **Document code:** A **doi:** 10.3969/j.issn.1007−7294.2026.06.006

0 Introduction

Ships and marine engineering structures are commonly subjected to variable amplitude loading such as wind, waves and currents, which may develop cracks due to fatigue damage during their service life. The fatigue crack propagation rate is greatly influenced by the interaction between variable amplitude loading, and the most common manifestations of the effect are crack propagation retardation effect due to tensile overload and the acceleration effect due to underload. Therefore, it is necessary to take the effect of variable amplitude loading into consideration when assessing the fatigue life of hull structures.

So far, the mechanism of fatigue crack propagation under variable amplitude loading has been studied, and a series of theoretical, experimental and numerical analysis results have been obtained[1−7]. Corigliano et al[8] presented a review of fatigue assessment approaches for welded marine joints and structures comprehensively, considering the recent advances in welding of dissimilar metals and autonomous welding.

Received date: 2025−12−16

Foundation items: Supported by the National Natural Science Foundation of China (51909198); the Natural Science Foundation of the Jiangsu Higher Education Institutions of China (23KJB580005); General Progarm of the Hubei Provincial Natural Science Foundation (2025AFB517)

Biography: DONG Qin (1988−), female, Ph.D., lecturer; DAI Qian-sheng (2002−), male, master's degree candidate; MAO Yi-xin (2002−), male, master's degree candidate; HU Yao-yu (1992−), male, Ph.D., lecturer; QIN Kai (1989−), male, Ph.D., lecturer, corresponding author, E-mail: qinkai@whut.edu.cn.

Numerous experimental studies on the overload phenomenon[9−11] showed that after the application of single tensile overload, crack propagation retardation phenomenon appears and the fatigue life is prolonged. Apparently, after the application of single tensile overload, a transient acceleration can be observed, followed by a sharp decrease to minimum, finally increasing to the steady state of constant amplitude loading.

Fatigue overload experiments on structural steel[12] and aluminum alloy[13−15] specimens with different thicknesses have shown that the larger the specimen's thickness is, the weaker the overload retardation effect is. The experimental results showed that the retardation cycles increased with the overload ratio to a certain extent. The crack propagation can be monitored experimentally by different ways, i.e. using infrared thermography or Digital Image Correlation (DIC)[16−17]. The acceleration effect caused by underload has been recognized by many scholars. Zheng[18−19] conducted fatigue crack propagation tests on cast aluminum alloys under underload, and the test results showed a very significant acceleration in the crack growth rate. Ding et al[20] found that the acceleration effect caused by underload is closely related to the residual tensile stress field near the crack tip by fatigue crack propagation tests on CT specimens of Q345R steel. Zhao et al[21] conducted fatigue tests on 7075-T651 aluminum alloy and Kalnaus et al[22] carried out fatigue crack propagation experiments on CT specimens of AL6XN stainless steel, and they both clearly emphasized that the crack growth rate showed a transient acceleration after the application of underload, but the acceleration degree was not large, so the effect of single underload on the acceleration of crack growth can be ignored under certain conditions. The underload can sometimes cause buckling like behavior. DIC technique was used to detect the strain patterns of AA5083 welded joints, indicating that a specimen tends to buckle under high compression load[23]. The study on effects of different combinations of overload/underload on the crack propagation behavior is also a focused problem in recent years. In a literature review by Skorupa[24] in 1998, it was pointed out that under the combined action of overload/underload, the retardation effect caused by tensile overload will be reduced accordingly with the magnitude and duration of the underload ratio. Schijve et al[25] conducted a crack propagation test on the central cracked specimens of D16 aluminum alloy under variable amplitude loading and found that the overload/underload combination exhibited the conventional retardation effect, while to some extent the applied underload weakened the retardation effect caused by tensile overload. There are many factors affecting the retardation effect, so it is necessary to systematically study the overload mechanism from multiple perspectives, such as crack closure[26], crack tip blunting[27], residual compressive stress[28], crack bifurcation[29−30] and so on to deepen the understanding of the overload mechanism. Qian et al[31] tried to study the crack tip stress field distribution after overload, and found that the effect of residual stress was reflected by stress cycle superposition. This superimposed effect, combined with fatigue accumulated damage, can be used to explain the intrinsic mechanism of crack growth after overload. The activation effect near the threshold value[32] has also been used to interpret the retardation effect after overload.

The Paris's law[33] was widely used in the mathematical description of fatigue crack growth due to its simplicity and convenience in application. However, it can only describe the elastic stage of fatigue crack growth. Wheeler[34] believed that the forward plastic zone formed at the crack tip by overloading makes it difficult for the crack to pass through under subsequent lower amplitude cyclic loads, leaving the crack tip surrounded by residual compressive stress, resulting in the overloading hysteresis effect. Based on the Wheeler model, Willenborg et al[35] proposed a model that considers the residual compressive stress introduced by overloading and predicts crack growth hysteresis using an analytical method. However, both the Wheeler model and the Willenborg model based on the residual compressive stress theory indicate that

fatigue crack growth immediately hysteresis after overloading, thus unable to explain the delayed hysteresis phenomenon. The improved McEvily model proposed by Cui et al[36−38] can cover the three stages of fatigue crack growth, and the improved McEvily model can explain the influence of many factors on crack growth, such as compressive fatigue, load sequence and stress ratio, etc., and has good application prospects.

Although many observations about overload have been repoted in the literature, the problem is still worth exploring because of the complicated mechanism behind it. It is an accepted fact that tensile overload may produce crack retardation while underload causes crack acceleration, but the intrinsic mechanism of the interaction between overload and underload has not been fully achieved. Therefore, it is necessary to investigate the crack growth behavior under tensile overload and underload systematically. A numerical analysis has been conducted to investigate the effects of different overload conditions on crack propagation behavior of AH32 steel in this work. The tensile overload ratios, overload-underload, underload-overload and underload were investigated in this study.

1 Numerical analysis

A detailed analysis of the crack tip parameters after the application of overload was carried out to explore the mechanical mechanism of the overload/underload effect by establishing a finite element model of propagating crack. The results of the elastic-plastic finite element analysis were used to illustrate the mechanical mechanism of the overload/overload effect, in order to provide a new idea for the evaluation of the crack propagation behavior of engineering components subjected to overload and underload.

1.1 Finite element model

The finite element software ABAQUS was used to establish the two-dimensional finite element model of the compact tension (CT) specimen to study the mechanical mechanism of the overload/underload effect. A half of CT specimen was modelled with CPS4 due to symmetry. The pre-crack length was 2 mm and the detailed geometry of CT specimen was shown in Fig. 1, with thickness of 12 mm. In order to obtain the high stress and strain gradients, refined elements were adopted near the crack tip, while coarse elements were performed far from the crack tip to improve computation efficiency. Considering the symmetry, the displacement in the y-direction was zero for each node located on the symmetric plane ($y=0$) ahead of the crack tip. The displacement in the x-direction was constrained for each node located at the upper top of the pin loading hole of the specimen. A rigid line was applied to simulate the contact between the crack surface and the symmetric surface, as displayed in Fig. 2. The rigid line and the crack surface were defined as the master surface and slave surface, respectively. The friction coefficient between the master surface and the slave surface was set to zero. A dynamic crack growth approach was taken and the node release method was applied to simulate the whole crack growth process. The crack growth process was carried out by debonding nodes one by one in the numerical model, from the same initial crack length to the same final crack length, different release rates could be adopted. Whether different release rates had an impact on the crack tip parameters and to what extent was the subject of this paper. Two cycles, three cycles, and four cycles were respectively selected to release one node, and each of the two cycles, three cycles, and four cycles was regarded as a block cycle. The node was released at the maximum load of the last cycle in each block cycle, and then the influence of the crack node release rate on the crack tip parameters was observed respectively. The displacement diagram of the first node after the crack tip for each node release technique is shown in Fig. 3.

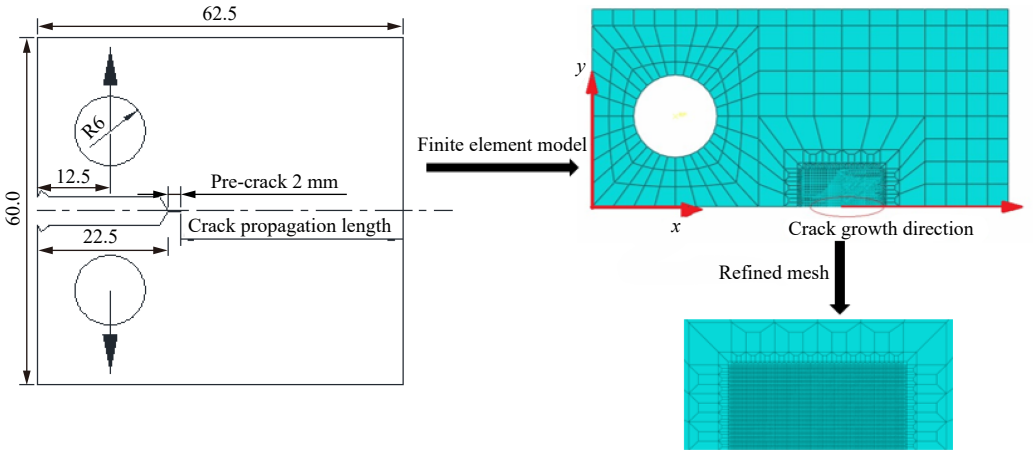


Fig.1 Detailed geometry and finite element discretization of CT specimen

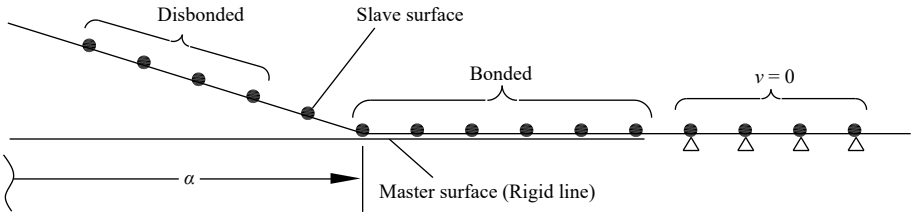


Fig.2 Diagram of node release method

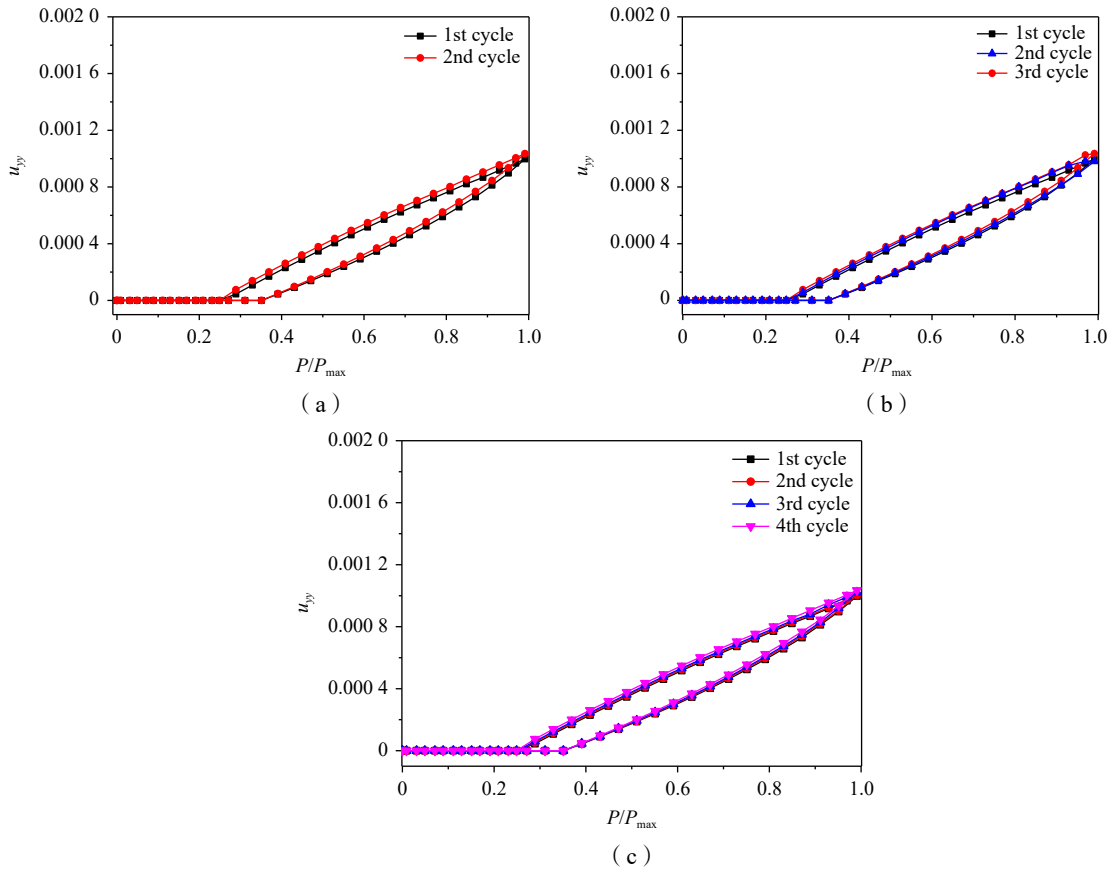


Fig.3 Displacement of the first node after the crack tip varying with different release rates

It can be seen from Fig. 3 that the release rates of different nodes have little effect on the displacement of the first node behind the crack tip. Therefore, two constant amplitude loading cycles need to be simulated

in order to obtain the stabilized cyclic stress-strain response. The crack tip fully propagates in the first loading cycle and leads to the redistribution of the stress/strain field around the crack tip. The second loading cycle is assumed to represent the stress and strain field ahead of the crack tip until the crack grows again by one element size.

1.2 Material model

The material used in the study was AH32 steel, a high strength steel which is mainly used for manufacturing hull and deck of ships. The Chaboche model was adopted to describe the nonlinear behavior of the material, which can describe the accumulative plasticity phenomena and ratcheting behavior at crack tip due to asymmetric cyclic loading. The initial yield surface was determined by applying the von Mises criterion as the yield criteria.

$$f(\sigma,\alpha,R,k)=J(\sigma-\alpha)-R-k\leqslant 0 \tag{1}$$

where σ is the stress tensor, α is the kinematic hardening variable, R is the isotropic hardening variable, k is the initial value of radius of yield surface, and J determines the scalar equivalent of the deviatoric stress state.

$$J(\sigma-\alpha)=\sqrt{\frac{3}{2}(\sigma'-\alpha'):(\sigma'-\alpha')} \tag{2}$$

where σ' and α' are the deviators of σ and α, and ':' represents the inner product of two tensors. The evolution of additive kinematic stress tensor α and isotropic stress R can be expressed as

$$\begin{cases}\dot{\alpha}=\sum_{i=1}^{n}\dot{\alpha}_i \\ \dot{\alpha}_i=C_i(\alpha_i\dot{\varepsilon}_p-\alpha_i\dot{p})\end{cases},\dot{R}=b(Q-R)\dot{p} \tag{3}$$

where C_i, α_i, b, Q are material and temperature dependent constants, and $\dot{p}$ is the accumulated inelastic strain rate defined by

$$\dot{p}=\sqrt{\frac{2}{3}\mathrm{d}\dot{\varepsilon}_p:\mathrm{d}\dot{\varepsilon}_p}. \tag{4}$$

Therefore, the model parameters of the full constitutive equations comprise Young's modulus E, Poisson's ratio ν, initial yielding stress k, kinematic hardening constants C_i and α_i, isotropic hardening constants b and Q. The parameter values of the Chaboche model obtained by optimizing the uniaxial fatigue test data of AH32 steel are shown in Tab. 1, which is capable of capturing the cyclic mechanical properties and the ratcheting behavior at the crack tip.

Tab.1 Material properties of the Chaboche model for AH32 steel

Material	E/GPa	ν	Q	b	c_1	α_1	c_2	α_2	c_3	α_3
AH32	206	0.3	72	8	314 310	800	28 071	321	1950	0

1.3 Verification of the accuracy of the finite element model

To verify the rationality of the Chaboche combined model material parameters, finite element calculations were conducted with a stress ratio $R=0.1$ and an applied maximum load $P_{\max}=35$ kN. The calculated nominal stress-strain curve was compared with the experimental nominal stress-strain curve, which is the work of the same team[39], as shown in Fig. 4. It can be seen that the

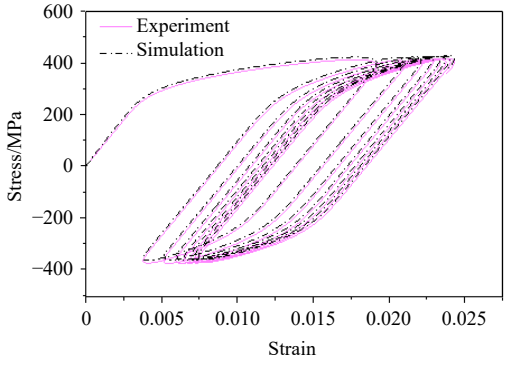


Fig.4 Comparison of cyclic nominal stress-strain curves

experimental nominal stress-strain curve is basically consistent with the stress-strain curve obtained from the finite element calculation, which proves that the material parameters selected in this model can more accurately reflect the stress-strain law of the material.

2 Study of the crack propagation behavior after tensile overload

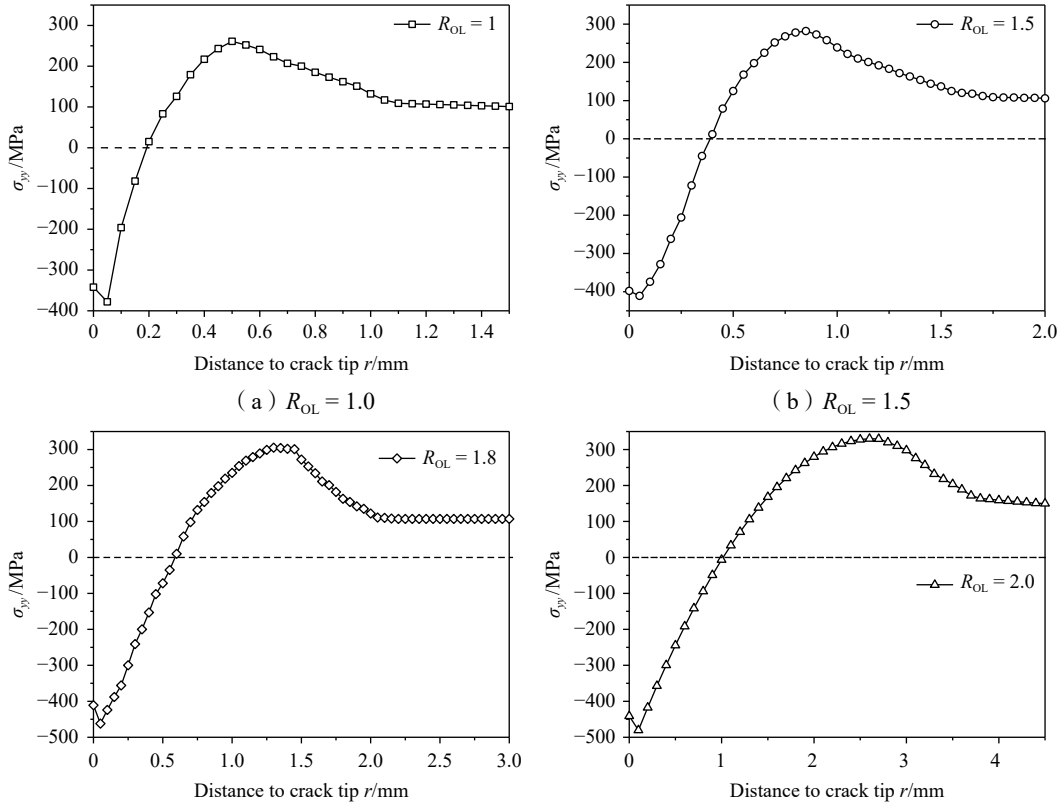
In order to study the crack propagation behavior after tensile overload, the stress-strain distribution near the crack tip after applying an overload was obtained, a single tensile overload corresponding to Tab. 2 was applied to the finite element model when the crack grows to $a=2.5$ mm, in which, P_{max} is the maximum applied load, R is stress ratio, R_{OL} is overload ratio, P_{OL} is the applied overload load.

Tab.2 Loading conditions

	P_{max}/kN	R	R_{OL}	P_{OL}/kN
Case I	35	0.3	1	35
Case II	35	0.3	1.5	52.5
Case III	35	0.3	1.8	63
Case IV	35	0.3	2	70

2.1 Crack tip stress field after tensile overload

Fig. 5 presents the distribution of the normal stress, σ_{yy}, at the crack tip in the $y=0$ plane at zero applied load after applying different tensile overload ratios, where $R_{OL}=1$ indicates the constant amplitude loading. It can be observed that a steep increase is followed by a continuous decrease in stress σ_{yy}, where overload ratio is the key parameter. It is evident that there is large compressive residual stress near the crack tip region, and the compressive residual stress is larger with increasing overload ratio. With the increase of distance to the crack tip, the compressive residual stress tends to decrease and gradually transforms into tensile residual stress after a certain range. The tensile residual stress eventually tends to zero when it continues to move away from the crack tip.



（a）$R_{OL}=1.0$ （b）$R_{OL}=1.5$

（c）$R_{OL}=1.8$ （d）$R_{OL}=2.0$

Fig.5 Stress distribution at crack tip under different overload ratios

To quantitatively study the relationship between crack tip stress distribution and tensile overload, the characteristic parameters of residual stress distribution at the crack tip are listed in Tab. 3.

Tab.3 Characteristics of crack tip stress field distribution under different tensile overload ratios

Overload ratio	Maximum compressive residual stress σ_{cm}/MPa	Compressive residual stress range r_c/mm	Maximum tensile residual stress σ_{tm}/MPa	Tensile residual stress range r_t/mm
$R_{OL}=1$	−376	0.21	262	0.32
$R_{OL}=1.5$	−413	0.34	283	0.58
$R_{OL}=1.8$	−464	0.65	302	0.86
$R_{OL}=2$	−498	1.02	334	1.73

It can be seen from Tab. 3 that the maximum compressive residual stresses at the crack tip under single tensile overload are −413 MPa, −464 MPa and −498 MPa, respectively, which are greater than the residual stresses at the crack tip under constant amplitude loading (−376 MPa). Apparently, the larger the overload ratio is, the larger the maximum compressive residual stress is. This can be explained by the retardation effect after overload due to the reduction of effective stress intensity factor caused by the compressive residual stress at the crack tip, thus resulting in a lower fatigue crack growth rate. Compared with constant amplitude loading, the compressive residual stress range after tensile overload increases gradually from 0.21 mm to 1.02 mm at overload ratio $R_{OL}=2$. This is because that the new crack tip will enter the reverse yielding state after overload, and the reverse yielding is more obvious with the increase of the overload ratio. Different from the distribution law of compressive residual stress, there is a tensile residual stress distribution area with a peak of about 300 MPa in front of the crack tip after different tensile overloads. The tensile residual stress range is very close to the size of plastic zone at the crack tip. It is evident that there is consistency between the residual stress distribution and the deformation behavior at the crack tip, which is due to the fact that the residual stress field of the crack tip after tensile overload is essentially the result of the residual plastic deformation of the crack tip after overload. Therefore, the crack tip plastic zone mechanism and the crack tip residual stress mechanism, which respectively describe the shielding effect of the crack tip front region from the strain field perspective and the stress field perspective, can explain the retardation effect of crack growth after overload are essentially consistent.

2.2 Crack opening displacement after tensile overload

Fig. 6 displays the variation of crack opening displacement during a single tensile overload cycle for different overload ratios ($R_{OL}=1.5$, $R_{OL}=1.8$, $R_{OL}=2$).

It can be seen from Fig. 6 that the crack opening displacement coincides with the constant amplitude loading curve when the tensile load $P/P_{max}<1$, i.e., the crack opening displacement increases slowly initially, then grows linearly with P/P_{max} when the load exceeds a certain range, indicating that there is an obvious crack closure phenomenon. When the tensile load $P/P_{max}>1$, the crack opening displacement gradually shows an increasing trend with the increase of P/P_{max}. The increasing phenomenon of crack opening displacement is closely related to the plastic zone at the crack tip.

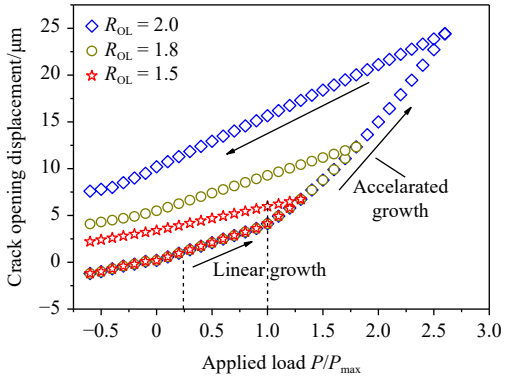


Fig.6 Crack opening and closing response under different tensile overload ratios

The size of the plastic zone at the crack tip before overload is small, and the shielding effect is weak. When the tensile load $P/P_{max} > 1$, the crack surface continues to open and a new plastic zone is formed in front of the crack tip. When the tensile overload is unloaded, residual crack opening displacement appears, and the residual crack opening displacement increases with the increase of tensile overload ratio. The residual crack opening displacement after unloading indicates that the tensile overload introduces a large plastic deformation near the crack tip region and prevents the elastic recovery of the surrounding material.

The crack opening profile evolution during a single tensile overload cycle with different overload ratios ($R_{OL}=1.5$, $R_{OL}=1.8$, $R_{OL}=2$) is shown in Fig. 7, and for comparison, the crack opening profile variation under constant amplitude loading is also given.

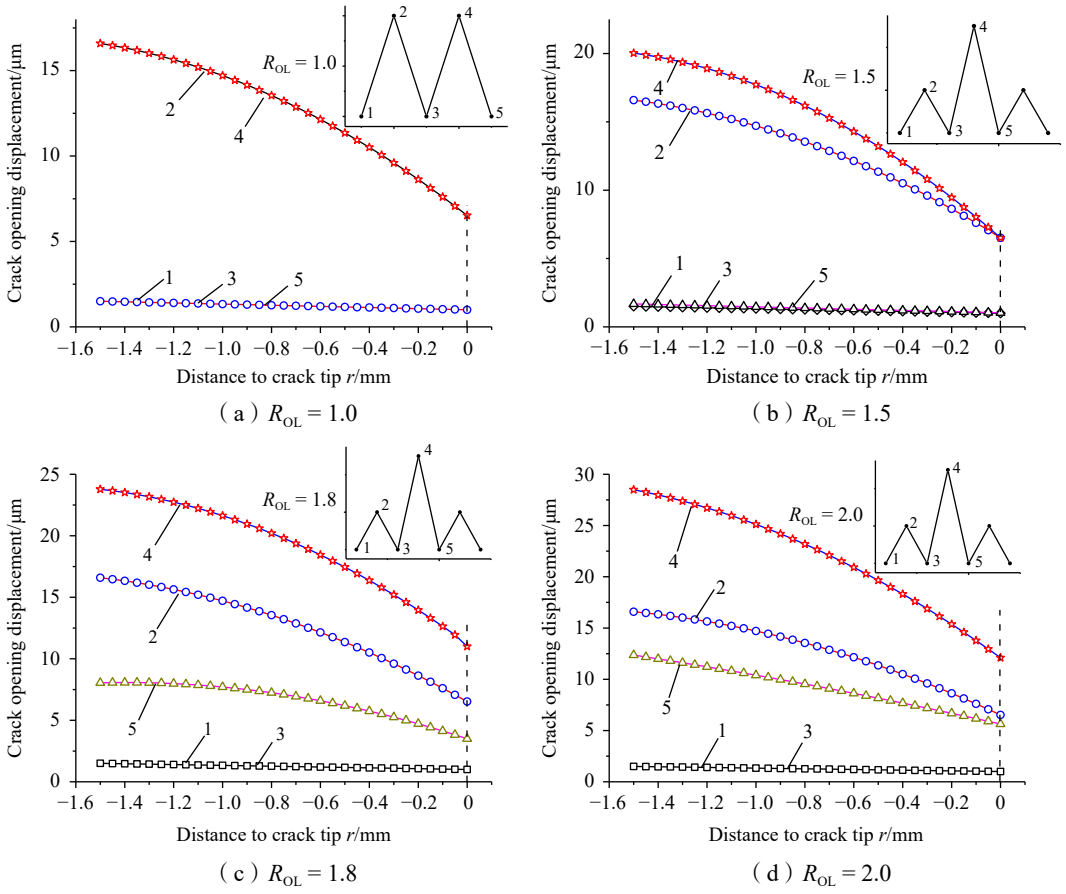


Fig.7 Variation of crack opening displacement under different overload ratios

As can be seen in Fig. 7, the crack surface is fully open when the constant amplitude is loaded to P_{max} before overload, and the crack surface still remains open when unloaded to the minimum load. The crack opening displacement of the node near crack tip contains both elastic and plastic deformation. When unloaded to the minimum load, the elastic deformation at the crack tip has recovered, while the residual plastic deformation keeps the crack surface open. After the application of tensile overload, the crack surface is slightly more open than under constant amplitude loading, and the crack opening displacement increases with the overload ratio. It can be seen that the shape of the crack tip changes considerably after the application of overload, which is consistent with the blunting effect caused by overload. The blunt crack tip weakens the stress concentration at the crack tip and is a cause of the retardation effect after overload. As the crack continues to grow, the displacement at the location where the tensile overload is applied is still open due to large non-returnable plastic deformation near the crack tip. The crack opening displacement increases with crack growth,

because the plastic damage accumulates during a number of cycles, and the accumulated value is greater than the elastic rebound and the reverse yielding caused by equivalent distal residual compressive stress.

3 Study of the crack propagation behavior after underload

In order to study the crack propagation behavior after underload, the stress-strain distribution near the crack tip after applying underload was obtained. Four typical loading conditions (single tensile overload (OL), single underload (UL), overload-underload (OL-UL) and underload-overload (UL-OL)) are shown in Fig. 8.

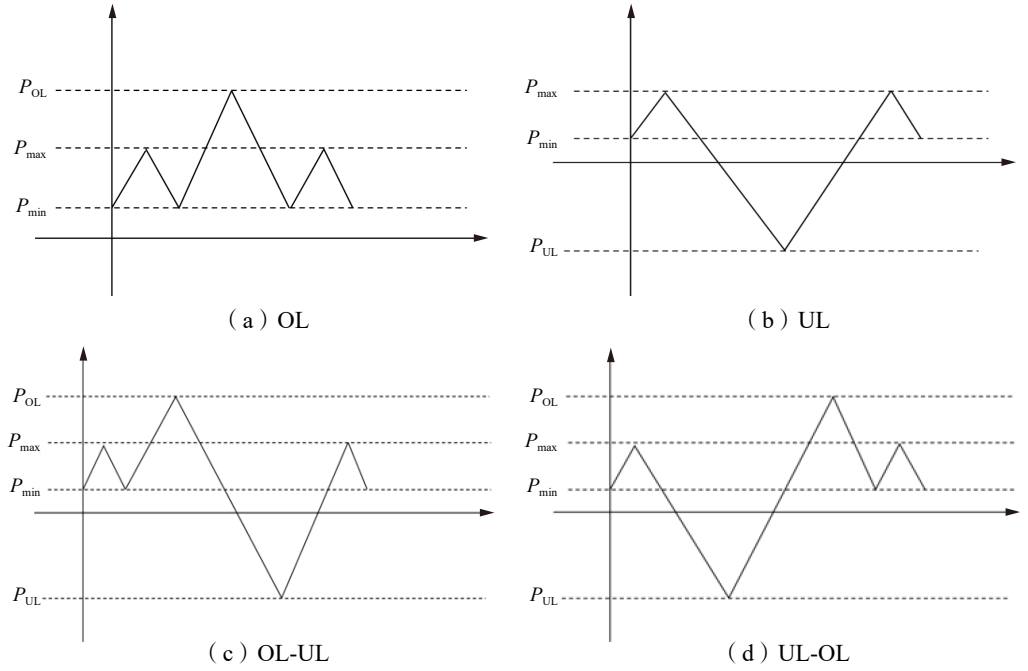
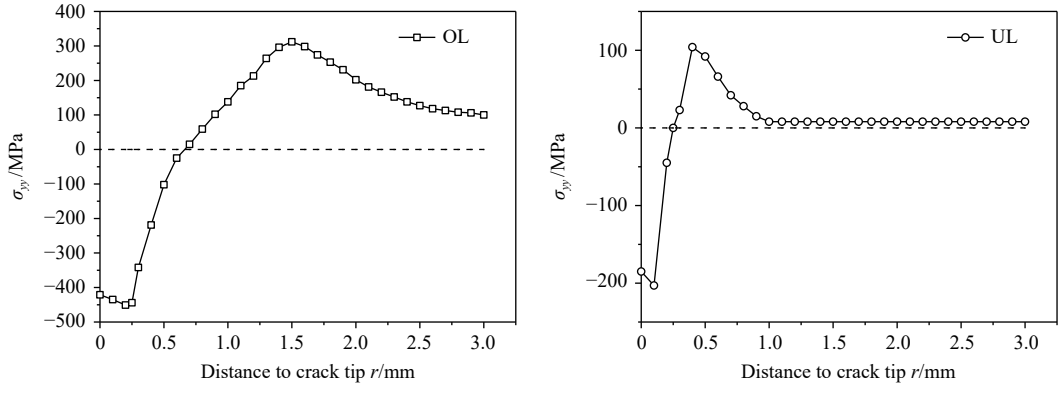
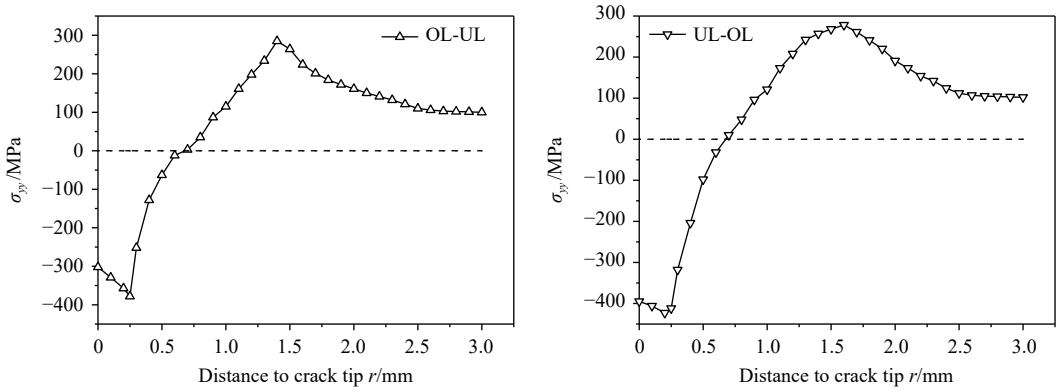


Fig.8 Typical load histories applied

3.1 Crack tip stress field after underload

Similar to the single tensile overload, the compressive residual stress field exists in a larger area in front of the crack tip after the overload-underload and the underload-overload, and is characterized by a gradient distribution, as shown in Fig. 9. It is evident that away from the crack tip, the compressive residual stress gradually decreases and converts to tensile residual stress, and eventually tends to zero. The value and range of compressive residual stress after a single underload are significantly smaller than those of the above three loading conditions.





（c）OL-UL （d）UL-OL

Fig.9 The crack tip stress field under different loading conditions

To quantitatively study the effect of different overload conditions on the residual stress distribution at the crack tip, the characteristic parameters of residual stress distribution at crack tip are listed in Tab. 4.

Tab.4 Characteristics of crack tip stress field distribution under different overload conditions

Overload conditions	Maximum compressive residual stress σ_{cm}/MPa	Compressive residual stress range r_c/mm	Maximum tensile residual stress σ_{tm}/MPa	Tensile residual stress range r_t/mm
OL	−452	0.61	303	1.82
UL	−205	0.15	104	0.17
OL-UL	−376	0.63	288	1.63
UL-OL	−433	0.54	279	1.61

From Tab. 4, it can be found that the maximum compressive residual stress at the crack tip after UL-OL (−433 MPa) is basically the same as that of a single tensile overload (−452 MPa), while maximum compressive residual stress at the crack tip after OL-UL is significantly reduced (−376 MPa). The compressive residual stress range is around 0.6 mm for all three overload conditions, and maximum tensile residual stresses in front of crack tip are also around 300 MPa, with no significant difference. Different from the above three overload conditions, the maximum compressive residual stress at the crack tip after a single underload is −205 MPa, which is slightly smaller than that under constant amplitude loading, and the compressive residual stress range is about 0.15 mm, which is consistent with that under constant amplitude loading. Comparison of the maximum tensile residual stress ranges under tensile overload, OL-UL and UL-OL with the crack tip plastic zone size under the same overload conditions has not shown the same variation trend. Namely, the results under tensile overload and UL-OL are similar, while the results under OL-UL are significantly smaller than the above, which may be due to the small differences in the maximum tensile residual stress ranges under the three overload conditions. The maximum compressive residual stress at the crack tip shows a similar variation trend with the plastic zone under different overload conditions, which is due to the significant plastic deformation of the material at the crack tip, and the residual stress distribution at crack tip under different overload conditions is the result of the residual plastic deformation near the crack tip after the overload.

The effects of different overload conditions on the stress distribution in front of the crack tip can be summarized as follows:

(1) A compressive residual stress field exists in the region near the crack tip, which is basically characterized by the following: a maximum compressive residual stress appears at the crack tip, and as the

distance to the crack tip increases, the compressive residual stress decreases and gradually transforms into tensile residual stress, and finally decreases to zero at the distal end. A single tensile overload introduces a larger compressive residual stress field at the crack tip, and it increases with overload ratio, while a single underload reduces the crack tip compressive residual stress field. In addition, the distribution of the residual stress field at crack tip is also closely related to the overload sequence. The crack tip stress distribution after OL-UL and UL-OL is very similar to that of single tensile overload, but the maximum compressive residual stress at crack tip after OL-UL is significantly smaller than that of UL-OL.

(2) Residual stress distribution in the region near crack tip under different overload ratios and overload conditions are all the results of plastic deformation of the material near the crack tip during fatigue crack propagation, and the mechanism of residual stress at the crack tip and the mechanism of plastic zone at the crack tip controlling the transient crack growth behavior under variable amplitude loading are essentially the same.

3.2 Crack opening displacement after underload

Fig. 10 presents the variation of crack opening displacement during a whole loading cycle under four different overload conditions (single tensile overload, single underload, overload-underload and underload-overload).

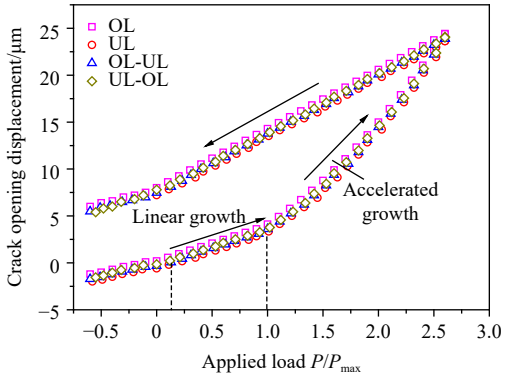


Fig.10 Crack opening and closing response under different overload conditions

In the initial tensile stage of single tensile overload, OL-UL and UL-OL, the crack opening displacement coincides with the constant amplitude loading curve when the tensile load $P/P_{max} < 1$, i.e., the crack opening displacement increases slowly initially, then grows linearly with P/P_{max} when the load exceeds a certain range, indicating that there is an obvious crack closure phenomenon. When the tensile load $P/P_{max} > 1$, the crack opening displacement gradually shows an increasing trend with P/P_{max} increasing. The increasing phenomenon of crack opening displacement is closely related to the plastic zone at crack tip. The size of the plastic zone at the crack tip before overload is small, and the shielding effect is weak. When the tensile load $P/P_{max} > 1$, the crack surface continues to open and a new plastic zone is formed in front of the crack tip. The variation curves of the three overload conditions (single tensile overload, OL-UL and UL-OL) almost coincide, and after unloading, a large residual crack opening displacement appears at the crack tip. Among which the residual crack opening displacement is the smallest under OL-UL, and those under UL-OL and single tensile overload are approximately equal and larger than that in the case of OL-UL. The smaller residual opening displacement under OL-UL is caused by underload, indicating that underload will reverse the tensile plastic strain introduced by tensile overload. There is almost no change in the crack opening displacement after a single underload, indicating that the underload has little effect on the deformation near the crack tip.

Fig. 11 presents the crack opening profile evolution during cyclic loading with four different overload conditions (single tensile overload, single underload, OL-UL and UL-OL). As shown in the figure, the crack surface is significantly opened under a single tensile overload, and after unloading the crack surface behind the crack tip is opened and the closure phenomenon disappears completely. Meanwhile the crack surface is

squeezed and approaches in reverse direction under single underload, and always remains closed. Under OL-UL, the tensile overload causes the crack surface to open and does not close after unloading, and the subsequent underload causes the crack surface to close again. Under UL-OL, the underload causes less change in the crack surface, which always remains closed, similar to the case of a single underload, and the subsequently applied tensile overload results in a significant crack surface opening. In summary, the crack surfaces after a single tensile overload, UL-OL and OL-UL are both completely open with blunting of the crack tip, and the crack surface after single underload is tightly closed with the crack tip remaining sharp, indicating that the crack face profile is closely related to the different overload conditions.

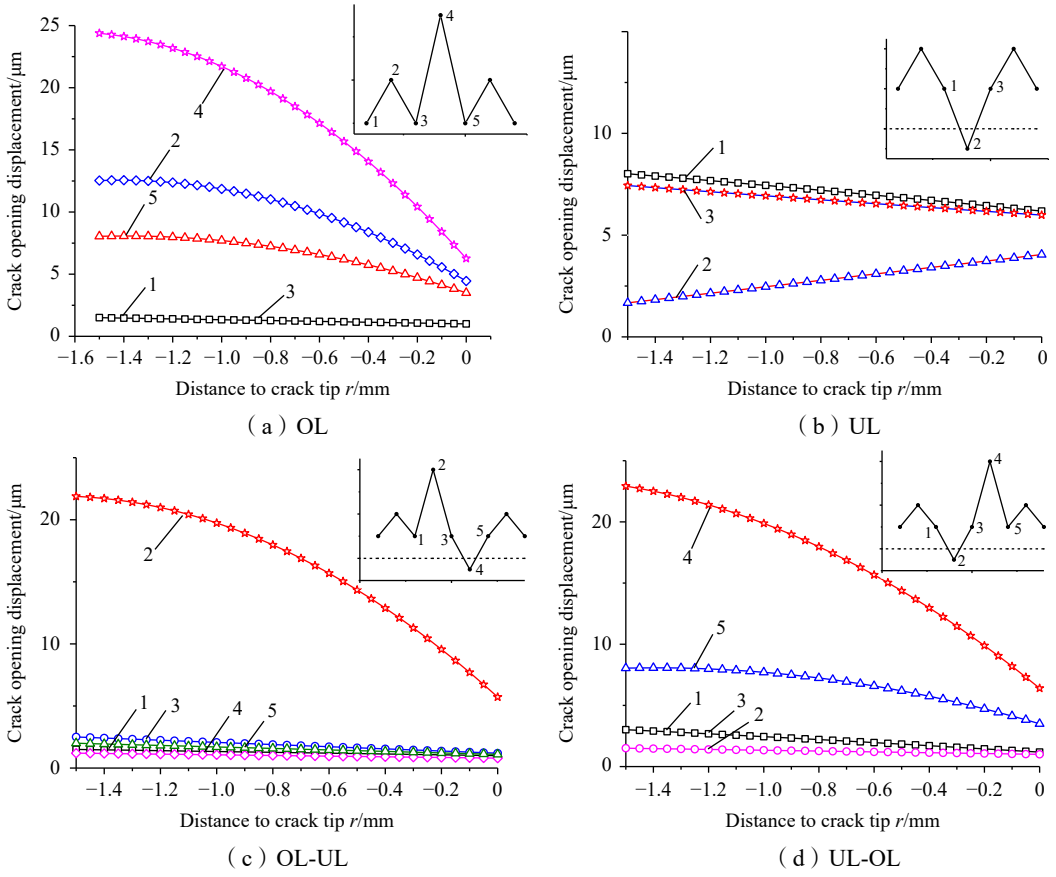


Fig.11 Variation of crack opening displacement under different overload conditions

The difference in effects of underload on crack growth rate among different overload conditions may be related to the crack face profile before underload. It can be found by analyzing the crack opening displacement that underload will squeeze the material near the crack tip, reduce the tensile plastic deformation at crack tip and promote crack closure. When the crack surface is tightly closed before underload and the crack tip is sharp (single tensile overload and UL-OL), the reduction effect of underload on residual strain of crack tip is smaller due to the disappearance of the crack tip singularity. When the crack surface is open before underload and the crack tip is blunted (OL-UL), the blunted tip introduces a notch effect that increases the local compressive stress at the crack tip, which in turn leads to a weakening of the retardation effect caused by tensile overload.

In summary, tensile overload introduces plastic deformation near the crack tip, and underload reduces the plastic deformation of the crack tip, but the degree of reduction is influenced by the blunted shape of the crack surface before underload, which is the main factor leading to the different crack growth behavior under

different overload sequences.

4 Conclusions

A numerical analysis has been implemented to investigate effects of different overload conditions on crack propagation behavior of AH32 steel. The tensile overload ratios, overload-underload, underload-overload and underload are explored in this study. Some conclusions can be drawn:

(1) Tensile overload introduces plastic deformation near crack tip, and underload reduces the plastic deformation of the crack tip, but the degree of reduction is influenced by the blunted shape of the crack surface before underload, which is the main factor leading to different crack growth behavior under different overload sequences.

(2) The residual stress distribution in the region near the crack tip under different overload ratios and overload conditions all result from plastic deformation of the material near the crack tip during fatigue crack propagation, and the mechanism of residual stress at the crack tip and the mechanism of plastic zone at the crack tip controlling the transient crack growth behavior under variable amplitude loading are essentially the same.

References

[1] Rong M Y, Dong Q, Xu G. Study of crack closure of hull plate under low cycle fatigue[J]. Journal of Marine Science and Engineering, 2022, 10(10): 1557.

[2] Xu S X, Tong Z, Cao J W, et al. Fatigue test and life prediction method of typical welded joints for marine aluminum alloy 5059[J]. Journal of Ship Mechanics, 2022, 26(12): 1823–1839.

[3] Huang X G, Wang Z Q, Zhang D H, et al. A low-cycle fatigue damage evolution model and its tolerance analysis of crack nucleation from notch[J]. Journal of Ship Mechanics, 2022, 26(3): 391–399.

[4] Xiong K, Deng J L, Pei Z Y, et al. Analysis of accumulative plasticity and fracture behavior of hull cracked plates subjected to biaxial low-cycle fatigue loading[J]. Journal of Ship Mechanics, 2022, 26(1): 113–124.

[5] Gai W Y, Gan J, Zhang S, et al. Experimental study on fatigue crack growth of compact tensile specimens under two-step variable amplitude loads with different cyclic ratios[J]. Journal of Ship Mechanics, 2021, 25(12): 1699–1707.

[6] Chen X Y, Liu N, Xu Z T, et al. Fatigue strength experiment and S-N curve fitting method of ship typical joints[J]. Journal of Ship Mechanics, 2021, 25(10): 1377–1389.

[7] Amirafshari P, Barltrop N, Wright M, K. Weld defect frequency, size statistics and probailistic models for ship structures[J]. International Journal of Fatigue, 2021, 145: 10669.

[8] Coriglano P, Crupi V. Review of fatigue assessment approaches for welded marine joints and structures[J]. Metals, 2022, 12: 1010.

[9] Liang H, Zhan R, Wang D P, et al. Effect of crack-tip deformation on fatigue crack growth: A comparative study under overload/underload conditions[J]. Theoretical and Applied Fracture Mechanics, 2022, 118: 103268.

[10] Neto D M, Borges M F, Antunes F V, et al. Mechanisms of fatigue crack growth in Ti-6Al-4V alloy subjected to single overloads[J]. Theoretical and Applied Fracture Mechanics, 2021, 114: 103024.

[11] Pommier S, Freitas M. Effect on fatigue crack growth of interactions between overloads[J]. Fatigue & Fracture of Engineering Materials & Structures, 2002, 25: 709–722.

[12] Shuter D, Geary W. Some aspects of fatigue crack growth retardation behavior following tensile overloads in a structural steel[J]. Fatigue & Fracture of Engineering Materials & Structures, 1996, 19(2-3): 185–199.

[13] Rodopoulos C A, Kermanidis A T. Understanding the effect of block overloading on the fatigue behavior of 2024-T351 aluminum alloy using the fatigue damage map[J]. International Journal of Fatigue, 2007, 29: 276–288.

[14] Borrego L P, Ferreira J M. Evaluation of overload effects on fatigue crack growth and closure[J]. Engineering Fracture Mechanics, 2003, 70(11): 1379–1397.

[15] Sander M, Richard H A. Lifetime predictions for real loading situations-concepts and experimental results of fatigue crack growth[J]. International Journal of Fatigue, 2003, 25: 999–1005.

[16] Erny C, Thevenet D, Cognard J Y, et al. Fatigue life prediction of welded ship details[J]. Marine Structures, 2012, 25: 13–32.

[17] Corigliano P, Cucinotta F, Guglielmino E, et al. Thermographic analysis during tensile tests and fatigue assessment of S355 steel[J]. Procedia Structural Integrity, 2019, 18: 280–286.

[18] Zheng X. Study on fatigue crack propagation and fatigue life for cast aluminum alloys under high-cycle & low-cycle interaction loading[D]. Nanjing: Nanjing University of Aeronautics and Astronautics, 2012.

[19] Zheng X, Cui H, Su X. Numerical modeling of fatigue crack propagation based on the theory of critical distances. Engineering[J] Fracture Mechanics, 2013, 114: 151−165.

[20] Ding Z Y, Wang X, Gao Z, et al. An experimental investigation and prediction of fatigue crack growth under overload/underload in Q345R steel[J]. International Journal of Fatigue, 2017, 98: 155–166.

[21] Zhao T W, Zhang J X, Jiang Y Y. A study of fatigue crack growth of 7075-T651 aluminum alloy[J]. International Journal of Fatigue, 2008, 30: 1169–1180.

[22] Kalnaus S, Fan F, Vasudevan A K, et al. An experimental investigation on fatigue crack growth of AL6XN stainless steel[J]. Engineering Fracture Mechanics, 2008, 75: 2002–2019.

[23] Corigliano P. On the compression instability during static and low cycle fatigue loadings of AA 5083 welded joints: Full-field and numerical analysis[J]. Journal of Marine Science and Engineering, 2022, 10: 212.

[24] Skorupa M. Load interaction effects during fatigue crack growth under variable amplitude loading-a literature review. Part I: Empirical trends[J]. Fatigue & Fracture of Engineering Materials & Structures, 1998, 21: 987–1006.

[25] Schijve J, Skorupa M, Skorupa A, et al. Fatigue crack growth in the aluminium alloy D16 under constant and variable amplitude loading[J]. International Journal of Fatigue, 2004, 26: 1–15.

[26] Sunder R. Extraction of crack closure component from threshold stress intensity[J]. Engineering Fracture Mechanics, 2022, 263: 108306.

[27] Sunder R, Biakow A, Eremin A, et al. Synergy of crack closure, near-tip residual stress and crack-tip blunting in crack growth under periodic overloads—A fractographic study[J]. International Journal of Fatigue, 2016, 93: 18–29.

[28] Ward-close C M, Blom A F, Ritches R O. Mechanisms associated with transient fatigue crack growth under variable amplitude loading: An experimental and numerical study[J]. Engineering Fracture Mechanics, 1989, 32(4): 613–638.

[29] Ward-Close C M, Ritchie R O. On the role of crack closure mechanisms in influencing fatigue crack growth following tensile overloads in a titanium alloy: Near-threshold versus higher ΔK behavior[A]. Mechanics of Fatigue Crack Closure[C]//America: ASTM STP 982, 1988: 93−111.

[30] Vecchio R S, Hertzberg R W, Jaccard R. On the overload induced fatigue crack propagation behavior in aluminium and steel alloys[J]. Fatigue & Fracture of Engineering Materials & Structures, 1984, 7(3): 181–194.

[31] Qian Y, Cui W C. An approach for predicting fatigue crack growth based on the cumulative damage theory and elasto-plastic stress field of crack tip[J]. Journal of Ship Mechanics, 2012, 16(8): 954–961.

[32] Sursh S. Micro-mechanisms of fatigue crack growth retardation following overloads[J]. Engineering Fracture Mechanics, 1983, 18(3): 577–593.

[33] Paris P C, Gomez M P, Anderson W E. A rational analytic theory of fatigue[J]. The Trend in Engineering, 1961(13): 9−14.

[34] Wheeler O E. Spectrum loading and crack growth[J]. Journal of Basic Engineering, ASTM, 1972, D94: 181−186.

[35] Willenborg J, Engle R M, Wood H A. A crack growth retardation model using an effective stress concept[R]. Technical Report Affdl-TM-71-1-FBR, Air Force Flight Dynamics Laboratory Report.

[36] Cui W C, Huang X P. A general constitution relation for fatigue crack growth analysis of metal structure[J]. Acta Metallurgica Sinica, 2003, 16(5): 342−354.

[37] Wang F, Chen F L, Cui W C. Applicability of the improved crack growth rate model and its parameters estimation method[J]. Journal of Ship Mechanics, 2010, 14(3): 252−262.

[38] Zhou C, Cui W C. Determination of fatigue crack growth rate using existing data[J]. Shipbuilding of China, 2003, 44(3): 74−79.

[39] Han J. Study on crack closure effect of low cycle fatigue cracked plate[D]. Wuhan: Wuhan University of Technology, 2017.

过载/低载对 AH32 钢疲劳裂纹扩展行为影响的数值分析

董　琴[1], 戴钱胜[2], 毛义鑫[2], 胡耀愚[3], 秦　恺[1]

（1. 高性能船舶技术教育部重点实验室(武汉理工大学), 武汉 430063; 2. 武汉理工大学 船海与能源动力工程学院, 武汉 430063; 3. 江苏科技大学 海洋装备研究院, 江苏 镇江 212003）

摘要: 本文研究不同过载条件对 AH32 钢裂纹扩展行为的影响包括拉伸过载比、过载-低载、低载-过载和低载。不同过载比和过载条件下裂纹尖端附近区域的残余应力分布都是疲劳裂纹扩展过程中裂纹尖端附近材料塑性变形的结果, 表明施加拉伸过载会延缓裂纹扩展, 而低载则会促进裂纹扩展。此外, 还观察到裂纹闭合水平随着过载比的增加而快速增加。最后, 在变幅载荷作用下, 裂纹尖端残余应力和裂纹尖端的塑性变形的控制瞬态裂纹扩展的行为机理基本相同。

关键词: 过载; 迟滞效应; 裂纹扩展; 裂纹闭合; AH32 钢

中图分类号: U668.2　　**文献标识码:** A

基金项目: 国家自然科学基金(51909198); 江苏省高等学校基础科学(自然科学)研究项目(23KJB580005); 湖北省自然科学基金一般面上项目(2025AFB517)

作者简介: 董　琴(1988−), 女, 博士, 讲师;

戴钱胜(2002−), 男, 硕士研究生;

毛义鑫(2002−), 男, 硕士研究生;

胡耀愚(1992−), 男, 博士, 讲师;

秦　恺(1989−), 男, 博士, 讲师, 通讯作者, E-mail: qinkai@whut.edu.cn。